ELSEVIER

Chemical Engineering Journal 137 (2008) 265–281

Chemical Engineering Journal

www.elsevier.com/locate/cej

Experimental study of bubble formation at metal porous spargers: Effect of liquid properties and sparger characteristics on the initial bubble size distribution

N.A. Kazakis, A.A. Mouza, S.V. Paras *

Laboratory of Chemical Process and Plant Design, Department of Chemical Engineering, Aristotle University of Thessaloniki, University Box 455, GR 54124 Thessaloniki, Greece

Received 5 January 2007; received in revised form 23 April 2007; accepted 24 April 2007

Abstract

This work is a study of the effect of liquid properties and pore size on the initial bubble size distribution of a bubble column equipped with fine pore sparger. Various liquids covering a wide range of surface tension and viscosity values are employed, while the gas phase is atmospheric air. A fast video recording technique is used for both the visual observations of the phenomena occurring onto the sparger and the bubble size measurements. A new correlation regarding the prediction of the *initial* mean Sauter diameter of bubbles formed from porous spargers at the homogeneous regime has been formulated and found to be in good agreement with available data. The experiments show that the mechanisms of bubble formation as well as the initial bubble size distribution depend strongly on the liquid properties, the sparger design and the gas flow rate.

Keywords: Bubble columns; Porous sparger; Homogeneous regime; Bubble size distribution; Sauter diameter; Coalescence

1. Introduction

Bubble columns are widely used as gas–liquid contactors in many applications such as absorption, blood oxygenation, fermentations, bio-reactions, coal liquefaction and waste water treatment. Due to their simple construction, low operating cost, high energy efficiency and good mass and heat transfer rates, bubble columns offer many advantages when used as gas–liquid contactors. However, their design and scale up is still a difficult task, due to the generally complex structure of the multiphase flow encountered in this type of equipment. In all these processes, bubble size is an important design parameter, since it dictates the available interfacial area for gas–liquid mass transfer. Also, in some applications the prediction of bubble size is crucial, e.g. in blood oxygenators, where large bubbles favor CO_2 removal, whereas small bubbles favor O_2 transfer, but it is more difficult to eliminate them in the debubbling section of the oxygenator [1].

Bubble size distribution depends extensively on column geometry, operating conditions, physical properties of the two phases and type of gas sparger [2]. Among the common gas spargers used, fine pore plate seems to be advantageous since bubbles created by this type of gas distributor are numerous and relatively small, offering a greater gas–liquid interfacial area for efficient mass transfer [3]. However, information related to the performance of this kind of sparger is quite limited.

From the two main flow regimes observed in bubble columns, i.e., the homogeneous and the heterogeneous regime, the homogeneous regime is more desirable for practical applications, because it offers a larger contact area [4]. In addition, it is preferable for applications where high gas flow rates may have undesirable implications and mainly for those involving sensitive materials. For example, in bioreactors, where cells and/or enzymes are shear sensitive, high gas flow rates must be avoided to provide a low shear rate environment [5]. Also, in blood oxygenators, high gas-to-blood flow ratio is one of the main causes of intravascular microemboli and organ injury during cardiopulmonary bypass and is associated with excessive hemolysis and protein denaturation [6].

In general, the *homogeneous* regime, encountered at relatively low gas velocities, is characterized by a distribution of

* Corresponding author. Tel.: +30 2310 996174; fax: +30 2310 996209.
E-mail address: paras@cheng.auth.gr (S.V. Paras).
URL: http://philon.cheng.auth.gr (S.V. Paras).

1385-8947/$ – see front matter © 2007 Elsevier B.V. All rights reserved.
doi:10.1016/j.cej.2007.04.040

Nomenclature

a	major bubble axis (m)
b	minor bubble axis (m)
d_b	bubble diameter (m)
d_p	pore diameter (m)
d_s	sparger diameter (m)
d_{32}	mean Sauter diameter (m)
F_σ	surface tension force (N)
F_d	drag force (N)
Fr	Froude number defined by Eq. (7)
g	acceleration of gravity (m/s^2)
k	minimum number of classes defined by Eq. (2)
n_i	number of bubbles in the dispersion of size class i
N	number of classes in bubble size distribution
Q_G	gas flow rate (m^3/s)
r_p	pore radius (m)
Re	Reynolds number defined by Eq. (9)
S	sample size
U_{GS}	gas superficial velocity based on the sparger surface (m/s)
W	average velocity of bubble expansion (m/s)
We	Weber number defined by Eq. (8)

Greek letters

ΔP	capillary pressure defined by Eq. (4) (Pa)
μ_L	liquid phase viscosity (Pa s)
ρ_L	liquid phase density (kg/m^3)
σ_L	surface tension (N/m)

small and almost identical bubbles and a radially uniform gas holdup [7]. However, when a porous sparger, which has a rather broad pore size distribution, is employed, the bubble diameters also follow a wide distribution even for the lowest gas flow rate. In this case, the homogeneous regime can be considered as the regime in which *discrete* bubbles are generated from the sparger and the gas holdup is linearly increasing with gas flow rate. This definition of the homogeneous regime [8–10] will be used throughout the present study.

An effective tool used for the study of bubble column hydrodynamics and their design is computational fluid dynamics

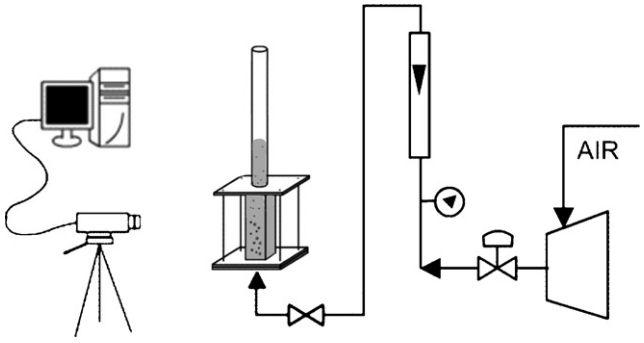

Fig. 1. Experimental set-up.

Table 1
Pore size range of a typical porous sparger (Mott Corp.)

Nominal pore size, d_p (μm)	Minimum pore diameter (μm)	Maximum pore diameter (μm)
40	3	70
100	5	500

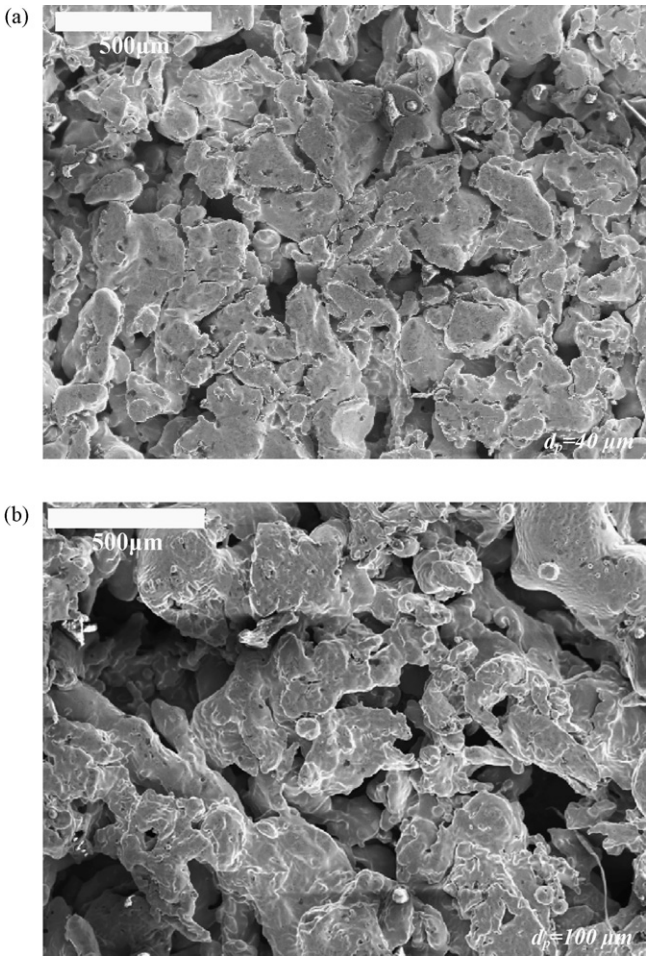

Fig. 2. Typical porous sparger images obtained by SEM (60× magnification): (a) d_p = 40 μm and (b) d_p = 100 μm.

Table 2
Liquid phase properties at 25 °C

Index	Liquid phase	Viscosity, μ_L (mPa s)	Density, ρ_L (kg/m^3)	Surface tension, σ_L (mN/m)
w	Water	1.0	997	72
i1	Isobutanol 0.75% (v/v)	0.9	992	60
i2	Isobutanol 2.2% (v/v)	0.9	990	49
g1	Glycerin 33.3% (v/v)	3.6	1080	70
g2	Glycerin 50.0% (v/v)	6.2	1140	69
g3	Glycerin 66.7% (v/v)	16.6	1180	67

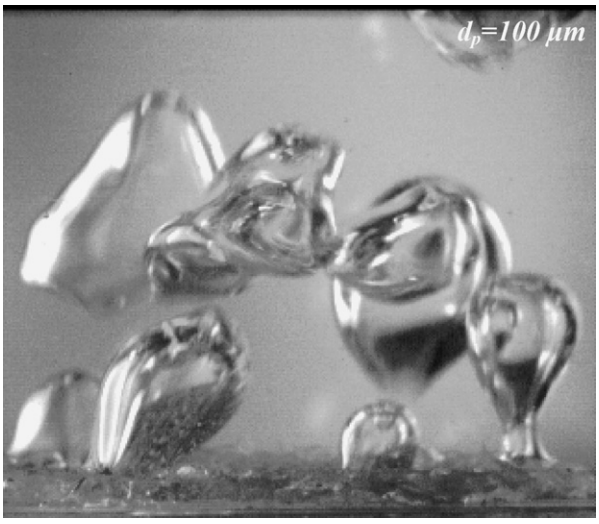

Fig. 3. Bubble formation for water (Q_G = 18.5 ml/s and d_p = 100 μm).

(CFD). An increasing number of papers deal with CFD application to bubble columns [4,11]. However, most of these studies assume a *monodispersed* bubble size distribution at the column entrance [12–16], a simplification that limits the validity of their models. Lehr et al. [13] pointed the importance of the *initial* size distribution by observing that different bubble sizes at the column entrance result in very different interfacial area densities available for heat and mass transfer. Consequently, it seems that, in order to develop reliable predictive tools for bubble column design, it is essential to be able to know the initial bubble size distribution, i.e., the distribution at the column entrance directly after the bubble detachment from the sparger, for various gas–liquid systems.

There are many studies in the literature dealing with the estimation of bubble size distribution or the mean Sauter diameter in bubble columns, but further detailed experimental and theoretical investigations are necessary. Most of these studies measure bubble size distribution at different heights of the column, away from the sparger area [2,3,17–20], or focus only on one gas–liquid system, without studying the effect of the physical properties on bubble size distribution [3,17,20,21]. The majority of the studies concern perforated plates or multi-nozzle spargers [17,18,21], while many of them base their statistics on samples with limited number of bubbles [2,18,20].

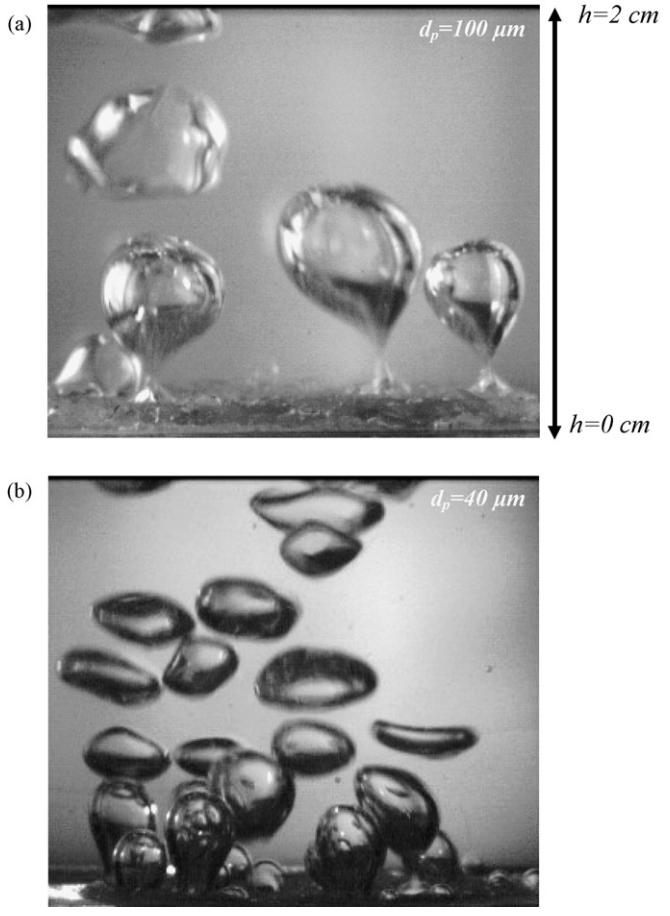

Fig. 4. Effect of pore size on bubble formation for water (Q_G = 10.9 ml/s): (a) d_p = 100 μm and (b) d_p = 40 μm.

To the authors' best knowledge, there is a limited number of studies on bubble size measurements in columns equipped with porous sparger [22–25]. These studies concern bubble size measurements away from the sparger [24,25], while many of these use non-coalescing liquids and assume that the size distribution remains practically unchanged along the bubble column [22,23]. In a previous work conducted in this laboratory, Mouza et al. [26] calculated bubble size distributions for various liquids at different heights from the porous sparger (3–40 cm) and showed the influence of viscosity and surface tension on bubble size. The lowest height at which the aforementioned investigators have

Table 3
Initial Sauter diameter (d_{32}) for the 100 and 40 μm spargers

Liquid phase	d_{32} (mm)					
	Q_G = 10.9 ml/s		Q_G = 14.7 ml/s		Q_G = 18.5 ml/s	
	d_p = 100 μm	d_p = 40 μm	d_p = 100 μm	d_p = 40 μm	d_p = 100 μm	d_p = 40 μm
w	7.3	5.1	7.4	5.2	7.7	–
gl	6.6	4.5	6.9	4.7	6.8	–
g2	6.3	4.3	6.6	4.3	6.8	–
g3	5.2	3.7	5.5	4.1	5.6	–
i1	6.0	4.4	5.6	4.3	5.5	–
i2	4.6	3.9	4.4	3.7	–	–

"–": not available.

studied the bubble size distribution is 3–5 cm above the sparger. However, almost all of them agree and accentuate that coalescence and breakage phenomena take place either directly onto or in the vicinity of the sparger surface. Consequently, ascending bubbles, after their detachment, interact and, thus, the initial size distribution is already altered, even few centimeters above the sparger. That is why Mouza et al. [26] noted that future experimental work must be focused on the phenomena occurring onto the sparger surface.

In the present work, new experimental data on initial bubble size distribution, namely the size distribution of the bubbles directly after their detachment from the sparger surface, and mean Sauter diameter at the homogeneous regime in a miniature bubble column equipped with two different fine-pore spargers, obtained from image analysis of fast video recordings, are reported. Various liquids covering a wide range of viscosity and surface tension are employed, while atmospheric air is used as the gas phase for all experiments. A correlation of general validity for the prediction of the Sauter diameter of the bubbles just after the detachment, in bubble columns with porous sparger operating at the homogeneous regime, has also been formulated.

2. Experimental set-up and measuring technique

The experimental set-up is illustrated in Fig. 1 and it consists of a small vertical rectangular Plexiglas® column (*cell*) with a square cross section of side length 4 cm and height 12 cm. To increase the total height of the column and to deter small bubbles returning to the sparger vicinity due to recirculation, a cylindrical Plexiglas® pipe (6.5 cm i.d. and 35 cm height) was also adjusted at the top of the column. The cell is equipped with appropriate rotameters for gas phase flow measurement and control. During the experiments, the gas is injected through a gas sparger, i.e., a round metal porous disc, 2.5 cm diameter, installed at the centre of the bottom plate. In the present experiments, two 316L SS porous discs (Mott Corp.) with nominal pore size of 40 and 100 μm were alternatively used as gas spargers.

The pore size range, given by the manufacturer of the above porous discs, is presented in Table 1. It is noted that the 100 μm sparger has a very broad pore size range and much larger pores compared to the 40 μm sparger. In order to confirm this difference, images were also obtained by scanning electron microscopy (SEM) (Fig. 2). It is easily observed that pores are of irregular shape and of non-uniform size and also that in the 40 μm sparger, pores are much smaller and more uniform compared to the 100 μm sparger, which indeed has a very broad pore size range.

All the experiments were conducted at ambient pressure and temperature conditions ($25 \pm 1\,^{\circ}C$). The gas phase was atmospheric air for all runs, while several liquids, i.e., water and various aqueous glycerin and isobutanol solutions, covering a sufficiently wide range of viscosity and surface tension values (Table 2), were employed as liquid phase. The liquid phase viscosity is measured by a KPG® Cannon-Fenske (Schott) vis-

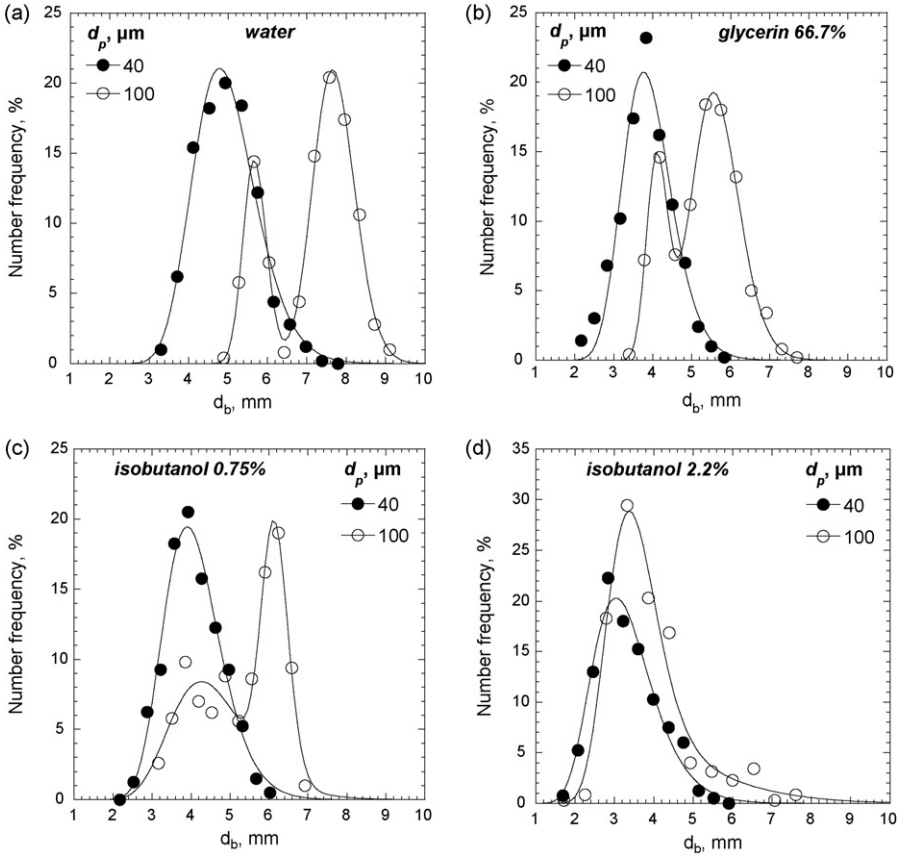

Fig. 5. Effect of pore size on initial bubble size distribution (Q_G = 14.7 ml/s): (a) water, (b) glycerin 66.7%, (c) isobutanol 0.75% and (d) isobutanol 2.2%.

cometer, while the surface tension is measured using the pendant drop method (KSV® CAM 200). Each experimental run is initiated by starting the gas supply and then filling the column with the appropriate liquid phase up to 30 cm above the sparger. This procedure was followed in order to eliminate the possibility of the liquid phase entering some pores and blocking them. All the experiments were performed with no liquid throughput.

An interesting general observation made during the experiments is that, even for relatively high gas flow rates, only a part of the porous sparger is activated (Fig. 3), a remark also made by Kaji et al. [8]. In addition, the number of the activated pores seems to depend on the gas flow rate, the mean pore size and the properties of the liquid phase, which is also pointed out by Bowonder and Kumar [27] and Houghton et al. [28].

A high-speed digital video camera (Redlake MotionScope PCI® 1000S) is employed for the bubble size measurements. The recorded images are also used to obtain an insight into the coalescence/breakage mechanisms occurring during bubble formation at the vicinity of the sparger. The camera is fixed on a stand very close to the area of observation in such a way that the test section is located between the camera and an appropriate lighting system placed behind a diffuser to evenly distribute the light. Although the imaging system used was capable of recording up to 1000 full frames per second (fps), a speed of 500 fps is considered a suitable recording rate for the present experiments. The shutter speed employed was of 1/5000. It must be also noted that the optical system offers a very narrow depth of field (few mm). The advantage of the above method is that it is non-intrusive and permits in situ measurements. Using appropriate software (Redlake MotionScope®) the size distribution of the bubbles formed, *directly* after their detachment from the porous sparger surface can be obtained from the recorded images for the various liquids and flow conditions examined. When the 100 μm sparger was used, the initial bubble size distribution was calculated for three different gas flow rates, whereas when the 40 μm sparger was employed, the initial bubble size distribution was determined only for the lower two, due to the large number of bubbles formed, leading to their overlapping at the focusing plane.

The calibration of the measuring system, needed to ensure the accurate measurement of the bubble size, is accomplished by measuring the known diameter of a cylindrical metal rod placed at the focusing plane. Subsequent image processing results in a sharp bubble–liquid interface. The bubbles were approximated by ellipses and the equivalent diameter of a sphere with the same volume as the ellipsoid was computed by the equation:

$$d_b = \sqrt[3]{a^2 b} \tag{1}$$

where d_b is the equivalent bubble diameter and a and b are the major and minor axes of the ellipsoid, respectively. Approximately 500 bubbles, just after their detachment from the porous sparger, were measured in each experimental run, a number considered to be adequate for statistical calculations [17,29]. The minimum number of classes required for the construction of the size distributions, k, was estimated using the Sturges' rule given by

$$k = 1 + \log_2 S \tag{2}$$

where S is the sample size (∼500 bubbles). The number of classes used for the construction of the distributions in the present study is 12 of equal interval, while it must be accentuated that the shape of the distributions remained practically unchanged even when a larger number of classes was used.

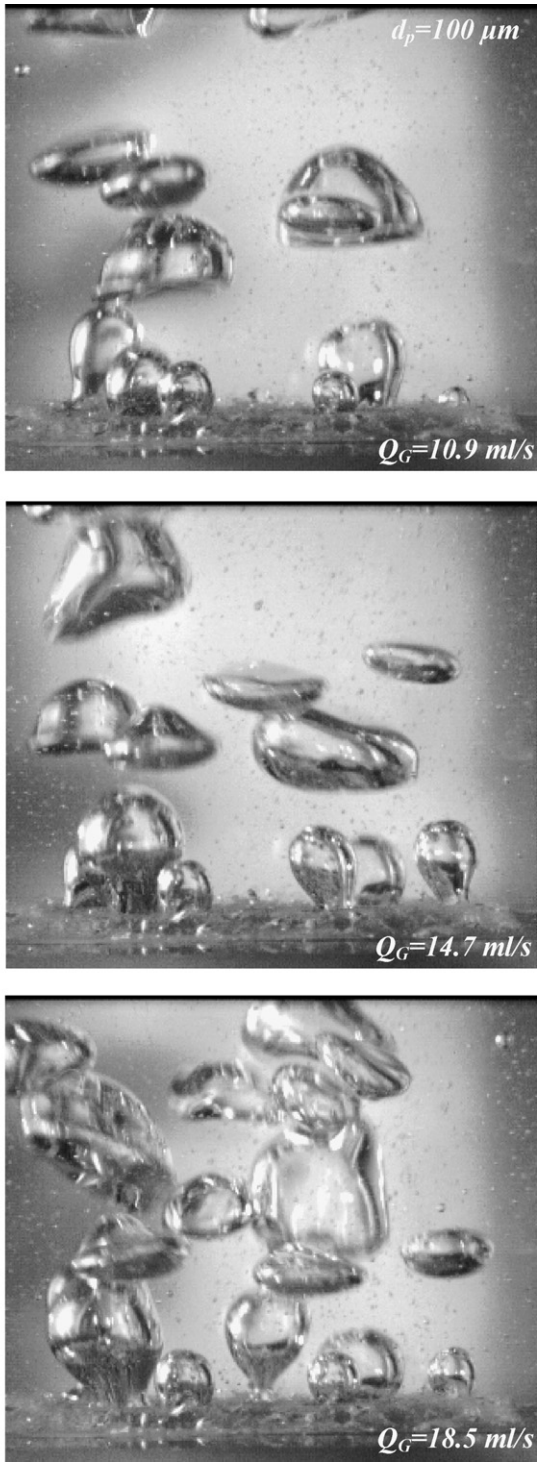

Fig. 6. Effect of gas flow rate on bubble formation for the glycerin 50.0% (d_p = 100 μm): (a) Q_G = 10.9 ml/s, (b) Q_G = 14.7 ml/s and (c) Q_G = 18.5 ml/s.

As previously mentioned, bubbles were considered ellipsoids. The spatial resolution of the measuring technique is approximately 60 μm, while the maximum uncertainty in measuring the length of each axis of the bubbles, due to unavoidable shadows at the bubble interface, is of the order of 250 μm. Considering all the above and the fact that the smallest bubbles measured in the present study are about 1.7 mm, it is estimated that the uncertainty of the measurements is less than 10%.

3. Results and discussion

In Table 3 the mean Sauter diameter (d_{32}) values for all the air–liquid systems tested are given. The empty cells in the table mean that the size distribution and the mean Sauter diameter could not be measured for these conditions, since the tracking of the bubble interface was impossible due to the large number of bubbles formed and their overlapping at the focusing plane. The mean Sauter diameter is defined as

$$d_{32} = \frac{\sum_i^N n_i d_{bi}^3}{\sum_i^N n_i d_{bi}^2} \tag{3}$$

where d_{bi} and n_i are the diameter and the number of the bubbles of size class i, respectively and N is the number of classes used for the distribution.

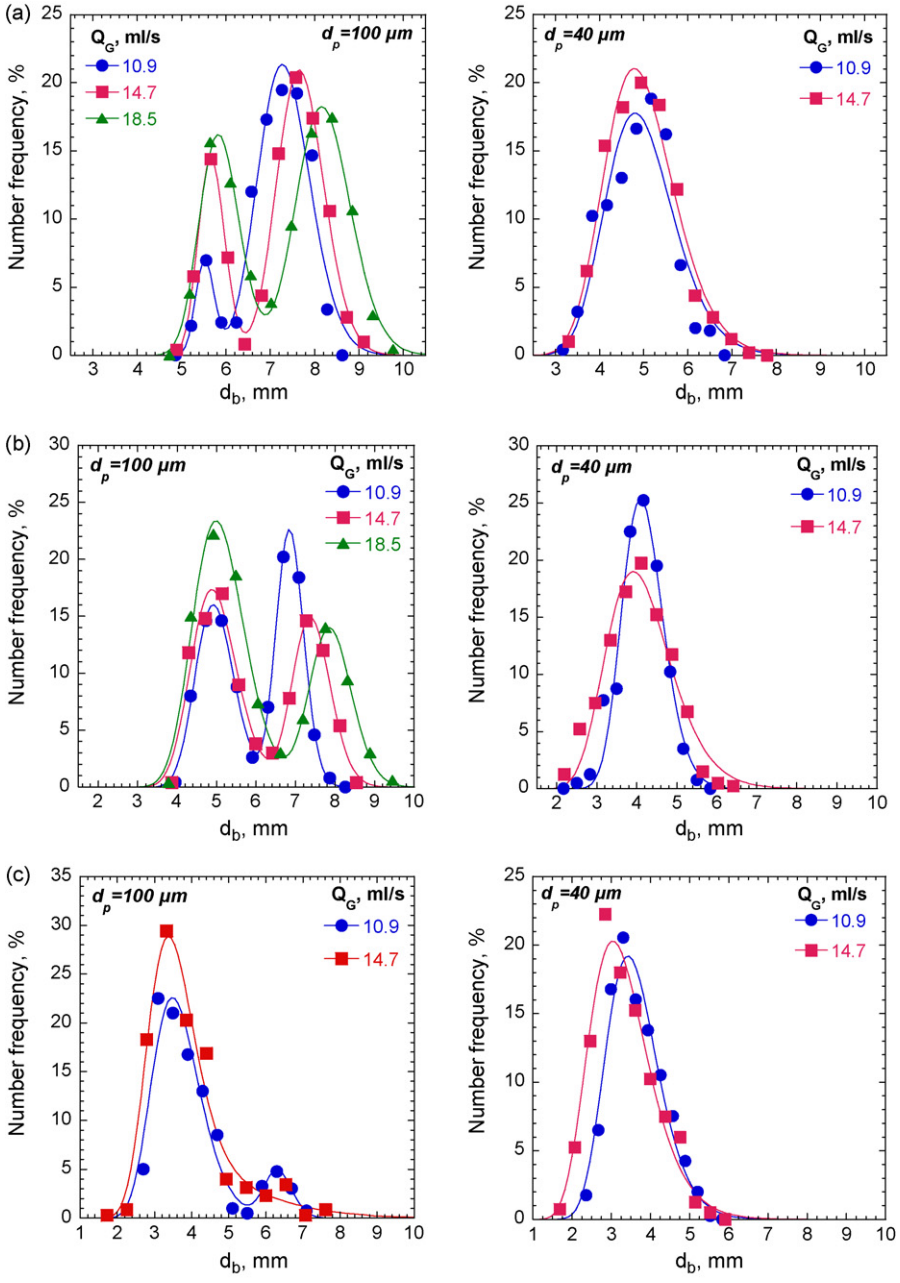

Fig. 7. Effect of gas flow rate on initial bubble size distribution: (a) water, (b) glycerin 50.0% and (c) isobutanol 2.2%.

3.1. Pore size effect

The pore size of the gas sparger seems to play an important role on the initial bubble size distribution. Fig. 4 illustrates two typical images of bubble formation at the same gas flow rate for water and for both spargers used. A first observation is that, for the same gas flow rate, the 40 μm sparger gives more numerous and much smaller bubbles than the 100 μm sparger. In addition, from Table 3 one can see that, when the 40 μm sparger is used, the mean Sauter diameter is 15–30% smaller than that of the 100 μm sparger.

This can be explained by assuming that the process of bubble formation starts with the pressure in the chamber below the sparger being equal to the hydrostatic pressure above it. As gas flows into the chamber, the pressure under the sparger increases. A bubble starts to form on a pore when the pressure under the pore overcomes the capillary pressure, which is actually the resistance to bubble formation [30]. The capillary pressure is given by

$$\Delta P = \frac{2\sigma_L}{r_p} \tag{4}$$

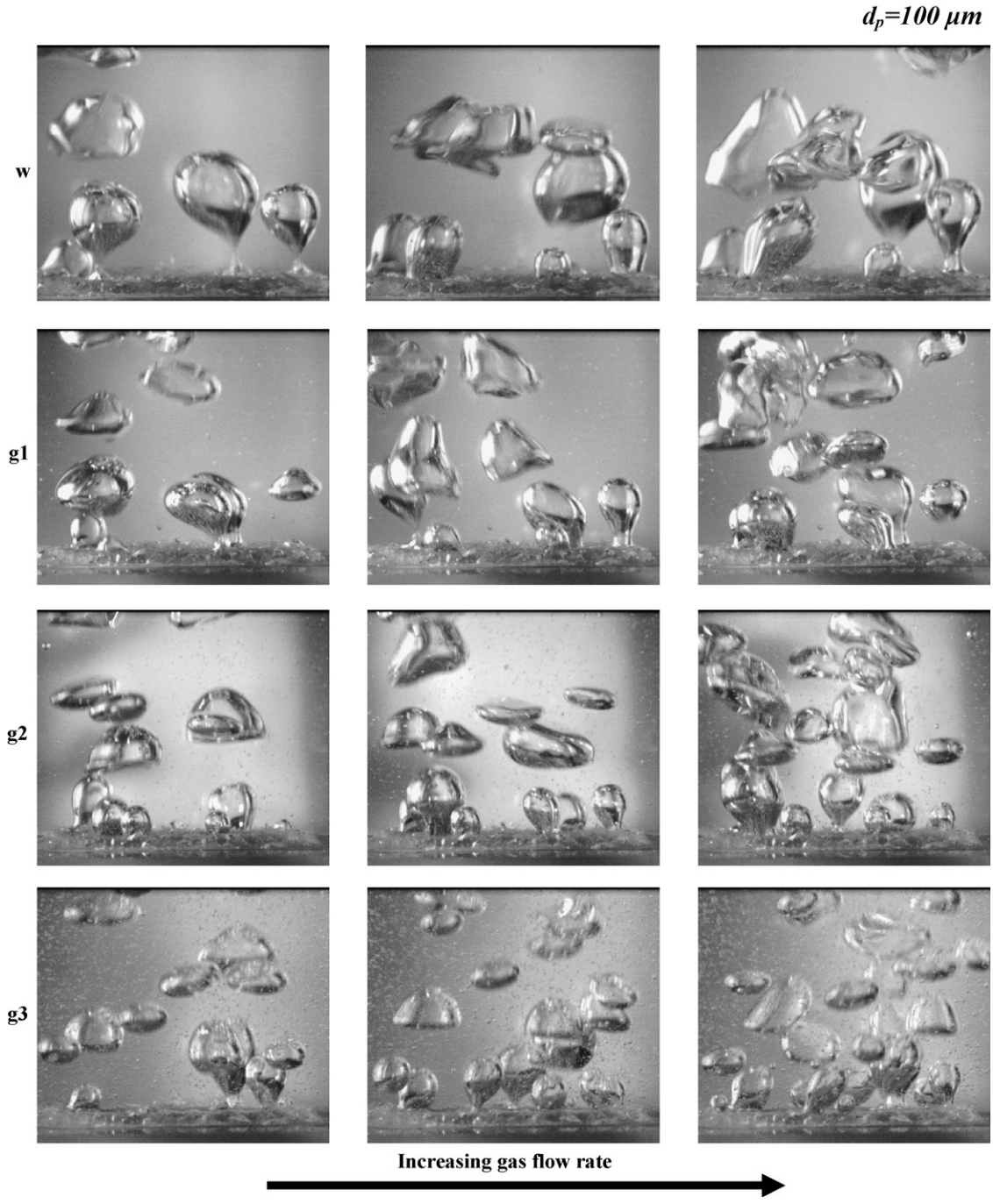

Fig. 8. Effect of viscosity on bubble formation for sparger with d_p = 100 μm.

where σ_L is the surface tension and r_p is the pore radius. In addition, as already discussed, the two spargers used have a very different pore size range and even though the minimum pore size is of the same order of magnitude for both of them, the maximum pore size of the 100 μm sparger is approximately seven times larger than that of the 40 μm sparger (Table 1). Consequently, since the 100 μm sparger has a broader size range with relatively large pores, capillary pressure is smaller for these pores and they are preferred as bubble formation sites [28,30], when this sparger is employed. This does not stand for the 40 μm sparger, where the pore size range is much narrower and gas is distributed more evenly across the sparger surface activating more pores and thus producing more numerous and smaller bubbles [8].

Fig. 5 illustrates the initial size distribution measured for the two spargers at the same gas flow rate for all the liquids tested. A first observation, which has been already discussed, is that the 40 μm sparger produces much smaller bubbles and, as expected, gives a log-normal distribution, which has been also observed by other investigators [2,22,26]. On the other hand, the 100 μm sparger generally gives a bimodal distribution, namely the summation of two log-normal distributions. This difference can be

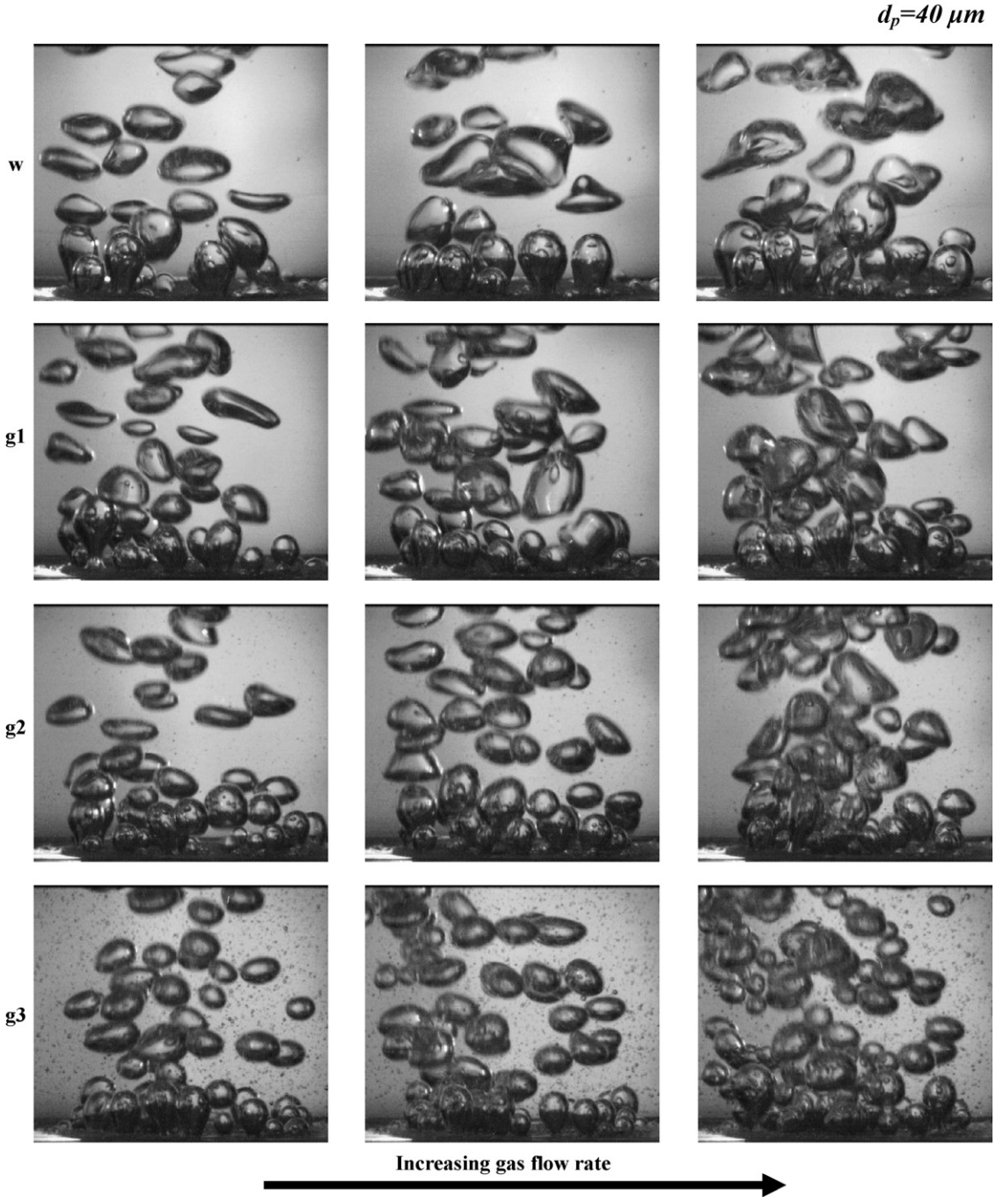

Fig. 9. Effect of viscosity on bubble formation for sparger with d_p = 40 μm.

ascribed to the pore size range of the two spargers, discussed previously. The two peaks shown in the distribution of the 100 μm sparger can be attributed to the broad size range of this sparger. More specifically, the first peak represents bubbles formed at larger pores while the second one corresponds to those formed at smaller ones that are also activated at each gas flow rate [28]. This is not the case for the 40 μm sparger, where the pore size range is much narrower and thus there are not large variations in bubble size.

3.2. Gas flow rate effect

Fig. 6 illustrates typical images of a glycerin solution during bubble formation for various gas flow rates when the 100 μm sparger is employed. It is observed that, as gas flow rate is increased, more pores are activated and hence more bubbles are formed. According to Eq. (4), the capillary pressure is smaller for larger pores. Consequently, when gas flow rate is relatively low, only the larger pores are activated, producing relatively large bubbles [28,30]. As the gas flow rate is increased, two are the main observations made for all liquids and for both spargers employed:

- some of the pores, which were already activated, produce slightly larger bubbles and
- other pores, even of smaller size, are also activated resulting in the formation of new smaller bubbles [28], since the gas flow rate increase induces an increase of the pressure under the porous sparger and thus the capillary pressure is overcome even for smaller pores [30].

The above can also be observed in Figs. 8, 9, 11 and 12.

In Fig. 7, the effect of gas flow rate on the initial bubble size distribution for both spargers used is illustrated. As gas flow rate increases the distribution curves become broader, a fact that is attributed to both the formation of new smaller bubbles from new activated pores and the formation of larger ones from already activated pores. Another observation is that the number frequency of the smaller bubbles, namely the bubbles belonging to the size classes on the left of the first peak, also increases with the gas flow rate for all liquids tested. In addition, according to Table 3, the mean Sauter diameter increases slightly with gas flow rate for the water and the glycerin solutions, while it decreases for the isobutanol solutions. This can be attributed to the fact that, in the low surface tension solutions the activation of new pores preponderates over the formation of larger bubbles from already activated pores leading to a reduction of the mean bubble size. This is also enhanced by the behavior of these solutions, which shows a coalescence inhibition [2]. The opposite stands for the other liquids employed, in which inter-

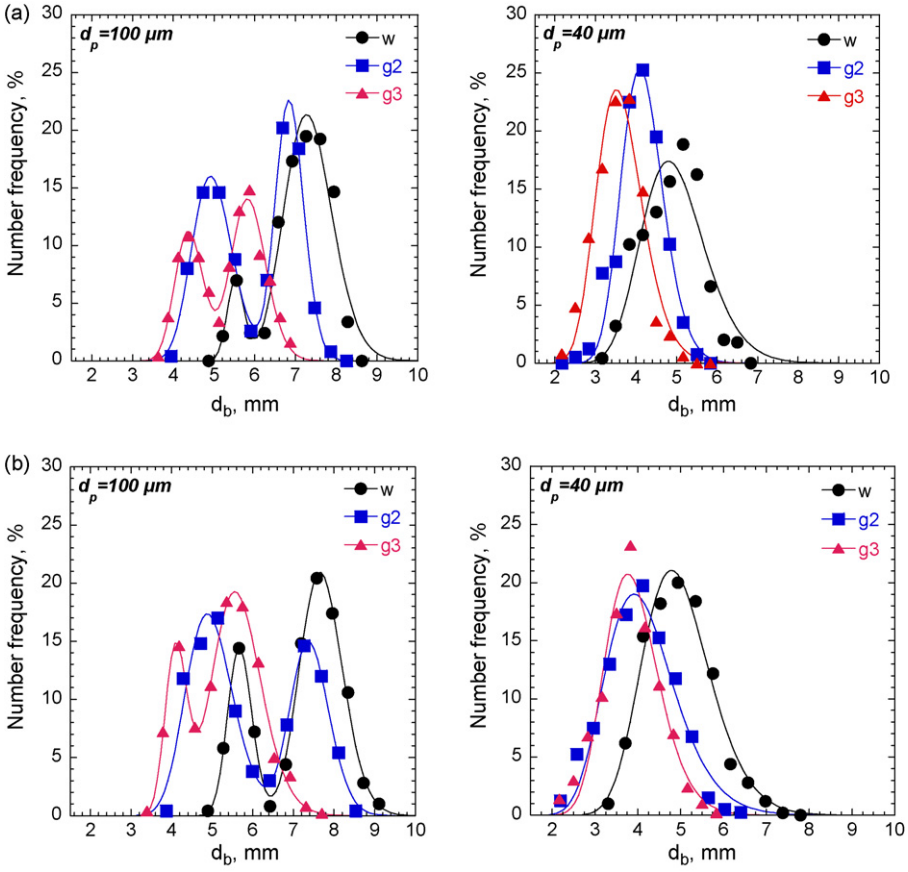

Fig. 10. Effect of viscosity on initial bubble size distribution: (a) Q_G = 10.9 ml/s and (b) Q_G = 14.7 ml/s.

actions between the bubbles onto the sparger surface are more pronounced.

3.3. Viscosity effect

Figs. 8 and 9 show the viscosity effect on the bubble formation, i.e., size and number of bubbles, from the 100 and 40 μm sparger, respectively, while Fig. 10 illustrates the viscosity effect on the initial size distribution. It is obvious that as viscosity increases, the size distribution curve shifts to lower bubble sizes. The same can be concluded from Table 3, where one can see that the mean Sauter diameter of the formed bubbles reduces as viscosity increases, which is consistent with the observations of Houghton et al. [28], who measured the largest bubble sizes in water and the smallest in an aqueous glycerin solution of high viscosity. This behaviour is ascribed to the activation of more pores for the same gas flow rate as viscosity increases, which leads to the formation of smaller bubbles. A question which arises is how the viscosity increase induces activation of more pores. In order to answer this question one has to take into account the forces acting on an under-formation bubble. The upward forces acting on a bubble during its formation are the buoyancy, the gas momentum force and the pressure force, while the downward forces are the drag force, the inertial force and the surface tension force [31]. At the instant just prior to detachment the upward forces are equal to the downward ones. The only force from the above which depends on the viscosity of the liquid phase is the drag force which is given by [31]

$$F_d = \frac{1}{2}\rho_L W^2 \frac{\pi d_b^2}{4}\left(\frac{24\mu_L}{\rho_L W d_b} + 1\right) \quad (5)$$

where W is the average velocity of bubble expansion, d_b the bubble diameter and ρ_L and μ_L are the liquid density and viscosity, respectively. According to Eq. (5), as viscosity increases, the drag force also increases retarding the growth stage of a bubble being formed at a pore. In addition, according to Loimer et al. [30] the pressure inside the pores is not the same everywhere across the sparger. Thus, since the gas flow rate through the sparger is constant and a bubble can not grow faster on an active site, gas is forced to flow to other directions inside the porous sparger increasing the pressure under other pores and activating them.

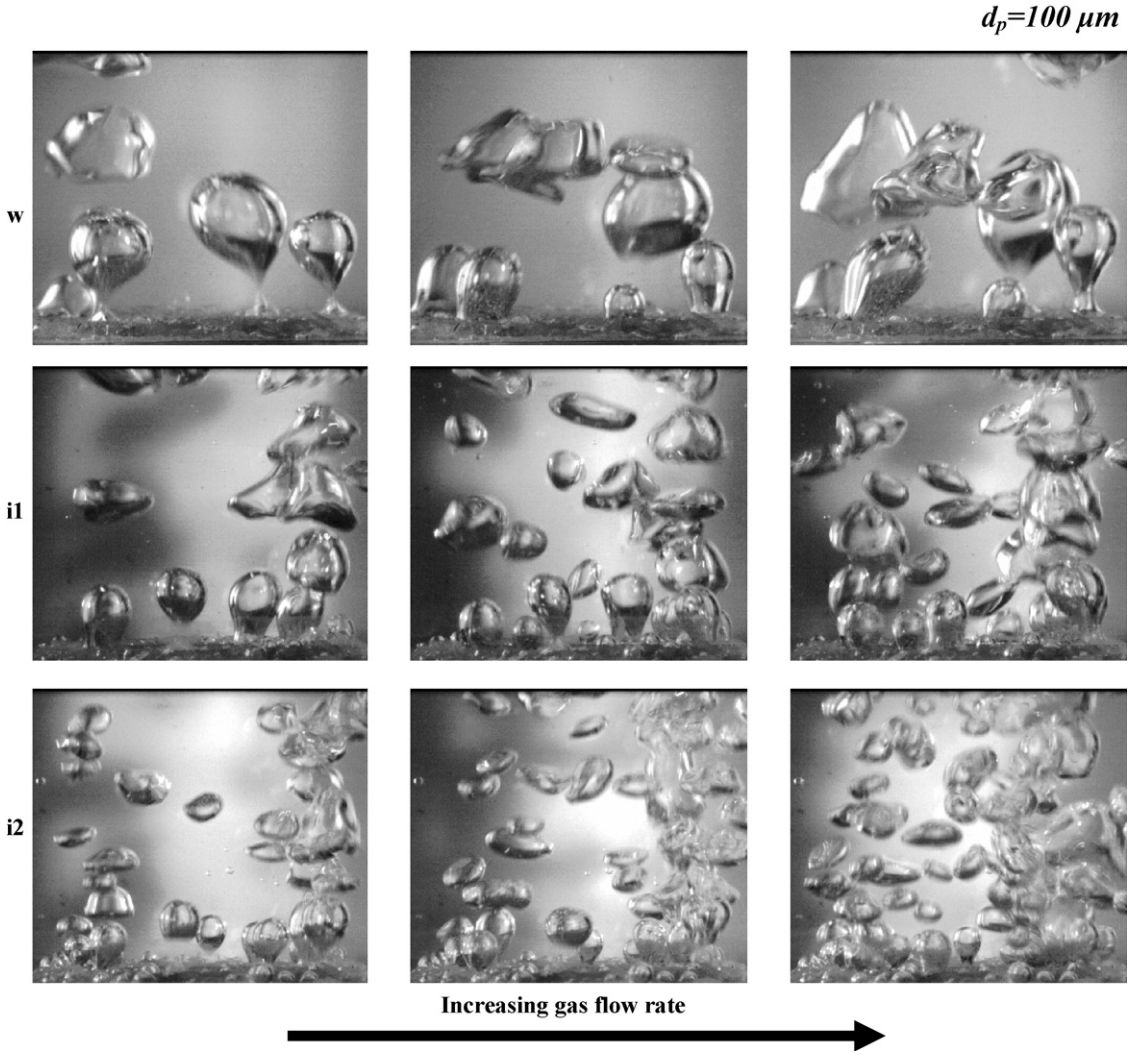

Fig. 11. Effect of surface tension on bubble formation for sparger with d_p = 100 μm.

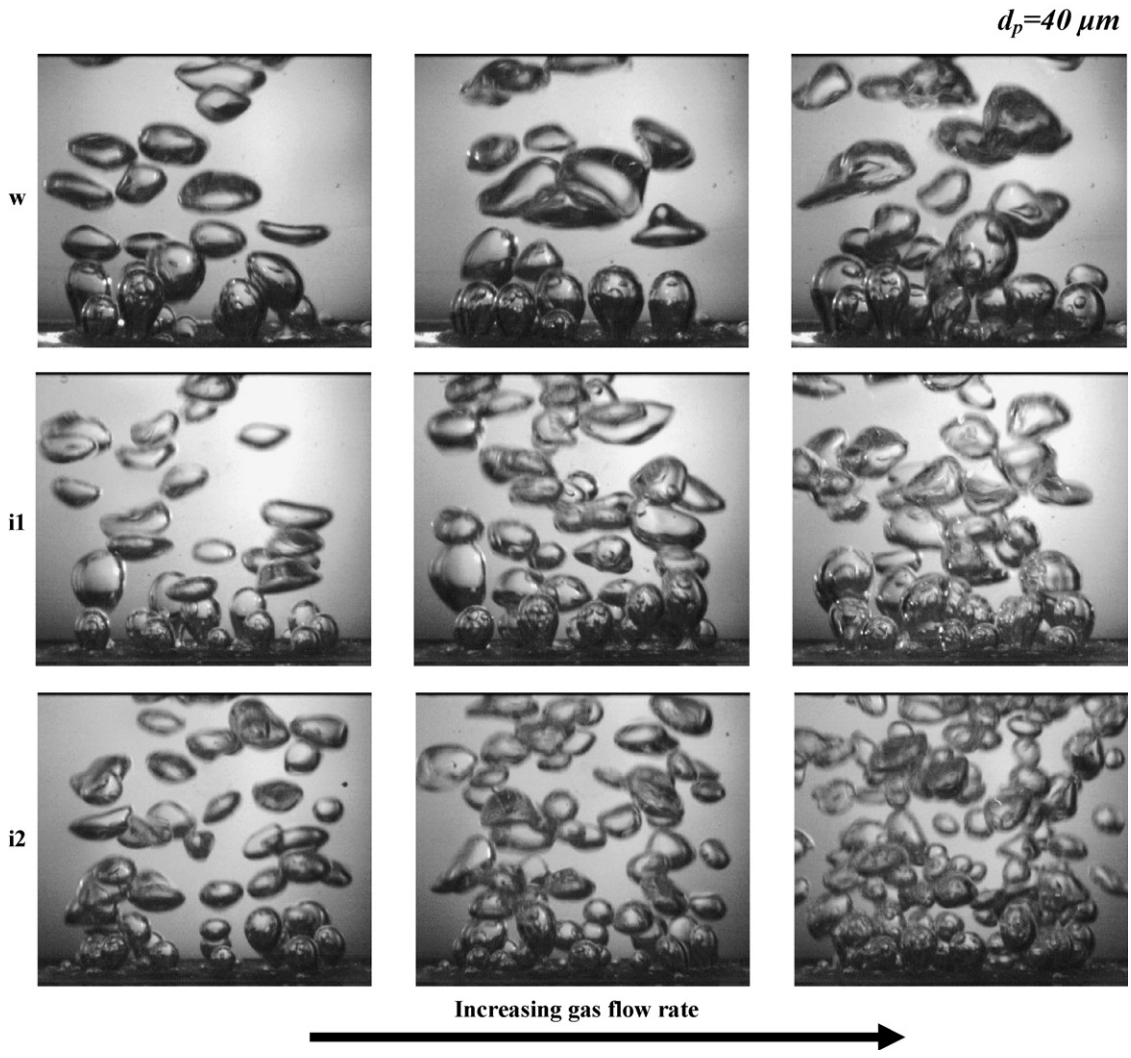

Fig. 12. Effect of surface tension on bubble formation for sparger with $d_p = 40\ \mu m$.

3.4. Surface tension effect

Figs. 11 and 12 show the effect of surface tension on the bubble formation, i.e., size and number of bubbles, at the 100 and 40 μm sparger, respectively, while Fig. 13 illustrates the surface tension effect on the initial size distribution. A first observation is that, as surface tension is reduced, more bubbles are formed and the initial size distribution shifts to lower sizes. Furthermore, from Table 3 it can be seen that the mean Sauter diameter is drastically reduced as surface tension decreases, an observation also made by other investigators [8,28]. According to Eq. (4), as surface tension decreases, the capillary pressure also decreases resulting in the activation of even smaller pores and the formation of more numerous bubbles [28]. The smaller mean Sauter diameter observed when liquids with low surface tension are employed, can be explained as follows: as already mentioned, one of the downward forces acting on a bubble during the expansion stage is the surface tension force given by

$$F_\sigma = 2\pi r_p \sigma_L \quad (6)$$

The surface tension force is the one which "holds" the bubble attached to the sparger as it grows. Consequently, as surface tension decreases, the surface tension force also decreases and thus bubble detachment occurs at smaller bubble diameter resulting in the formation of much smaller bubbles.

3.5. Bubble formation on porous sparger

Fig. 14 illustrates the bubble formation process on the porous sparger. Careful observation of the diameter of the under-formation bubble, before it starts to grow, indicates that a bubble on a porous sparger is not "fed" from an individual pore. On the contrary, it is produced by the joint action of many neighboring pores which actually act as a large one.

The incipient bubble diameter, i.e., the bubble diameter before it starts growing (Fig. 14), has been measured and found equal to about 4.8 mm while the resultant bubble after detachment is about 8 mm. In Fig. 15, the difference in the incipient bubble diameter between two bubbles growing at different sparger regions can be observed. The bubble on the left is the same mentioned earlier while the one on the right has an incip-

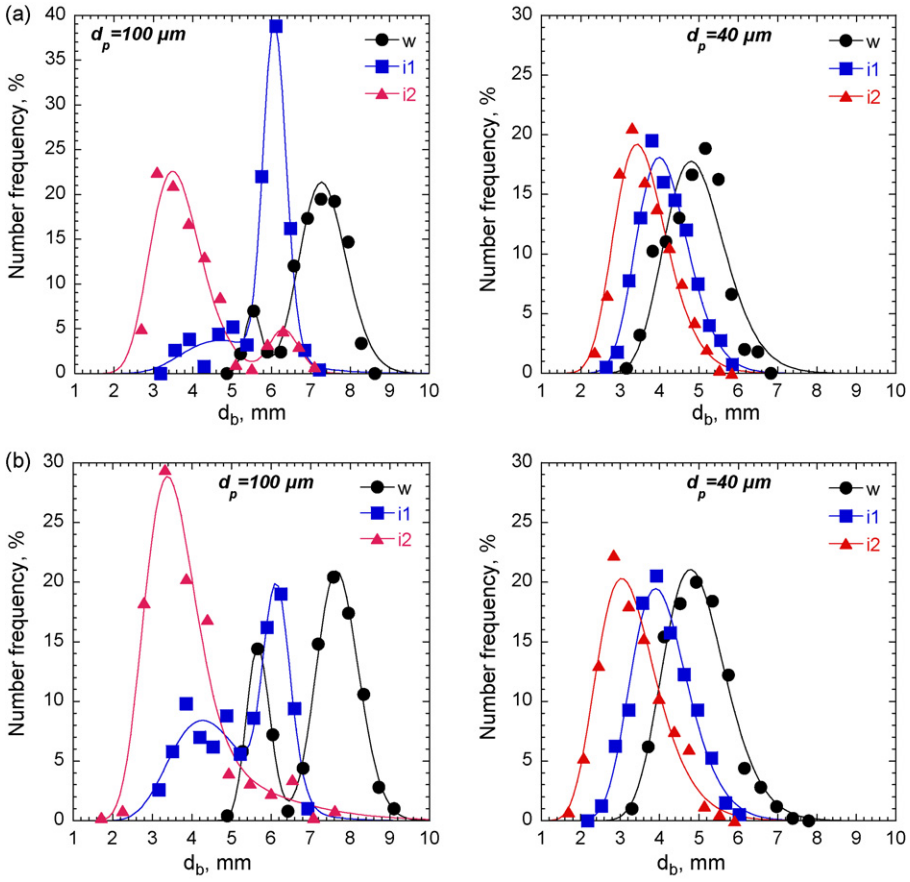

Fig. 13. Effect of surface tension on initial bubble size distribution for: (a) Q_G = 10.9 ml/s and (b) Q_G = 14.7 ml/s.

ient diameter, before the growth stage, about 3.3 mm and the resultant bubble is about 6 mm. Consequently, it seems that the different bubble sizes during bubble formation depend on the sparger area that the bubbles cover just after gas exits the porous sparger. It seems that pores which are very close can be activated together and simultaneously contribute to the growth of one bubble.

It must be noted that bubble formation is also influenced by the material of the porous sparger (glass, stainless steel, teflon, nickel, etc.) since it affects the contact angle [32]. In the present work, only stainless steel, a popular material for this type of distributor, porous spargers were employed. However, Koide et al. [25], who studied bubble formation at porous sparger, found that except in the case when the teflon porous plate was used as a distributor, the material used for the construction of the porous plate did not have an appreciable effect on the bubble formation behavior.

3.6. Bubble interactions

In a previous work conducted in this laboratory, Mouza et al. [26], not only concluded that the liquid properties influence coalescence/breakup mechanisms, but they also argued that bubble sizes in columns equipped with fine pore spargers depend mostly on phenomena that take place either directly onto or in the vicinity of the sparger region. That was also confirmed in the present work, since, during the experiments, many bubble interactions were observed either directly onto or near the sparger region for both spargers and for all liquids employed, with the exclusion of the isobutanol solutions. As already mentioned, coalescence is inhibited when these solutions are employed as the liquid phase. The same behavior is also observed when small quantities of salt or some organic liquids are added to water [23,33].

Bubble coalescence on the sparger surface is a phenomenon occurring not only at high gas flow rates, but even at very low ones. Fig. 16a illustrates the coalescence between two under-formation bubbles on the sparger surface, while Fig. 16b shows the simultaneous coalescence of three bubbles in the vicinity of the porous sparger.

Fig. 17 gives a comparison between the initial bubble size distribution (i.e., directly on the sparger) and the one obtained by Mouza et al. [26] (3–4 cm above sparger) for water, the 40 μm sparger and practically the same gas flow rate. It is obvious that the initial bubble size distribution of the present study is shifted to higher bubble size values. Since Mouza et al. [26] measured the bubble size distribution few centimeters above the sparger, it can be concluded that bubble breakage occurs in the vicinity of the sparger directly after bubble detachment. This claim is in agreement with visual observations conducted in the present study about 3 cm above the sparger, where bubble breakage found to take place in a great extent. Fig. 18

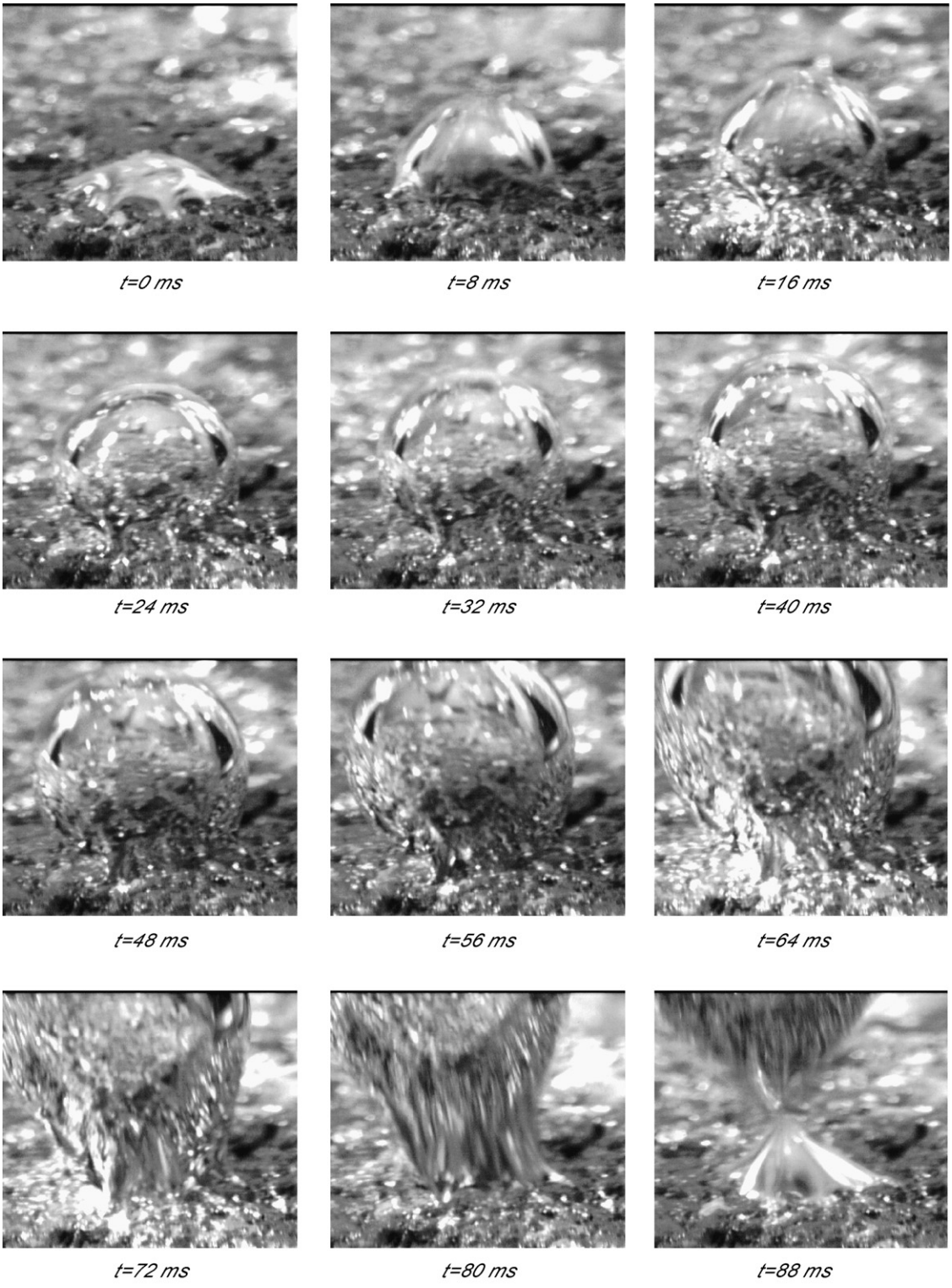

Fig. 14. Instances of a bubble formation.

illustrates the breakage of a large bubble into two daughter bubbles few centimeters (i.e., 3 cm) above the sparger. Furthermore, in some cases, especially when the glycerin solutions were employed, very small bubbles traveling inside the cell were also observed. These small bubbles could be the result of bubble breakage occurring inside the cell, since bubbles of that size are not produced from the sparger. It seems more possible that these bubbles are the result of a coalescence-linked breakup mechanism [34]. Tse et al. [34] observed that the coalescence of two bubbles can result in the formation of a smaller one and this breakage mechanism is more pronounced when the coalesced bubbles are large. From the above, it seems that inter-

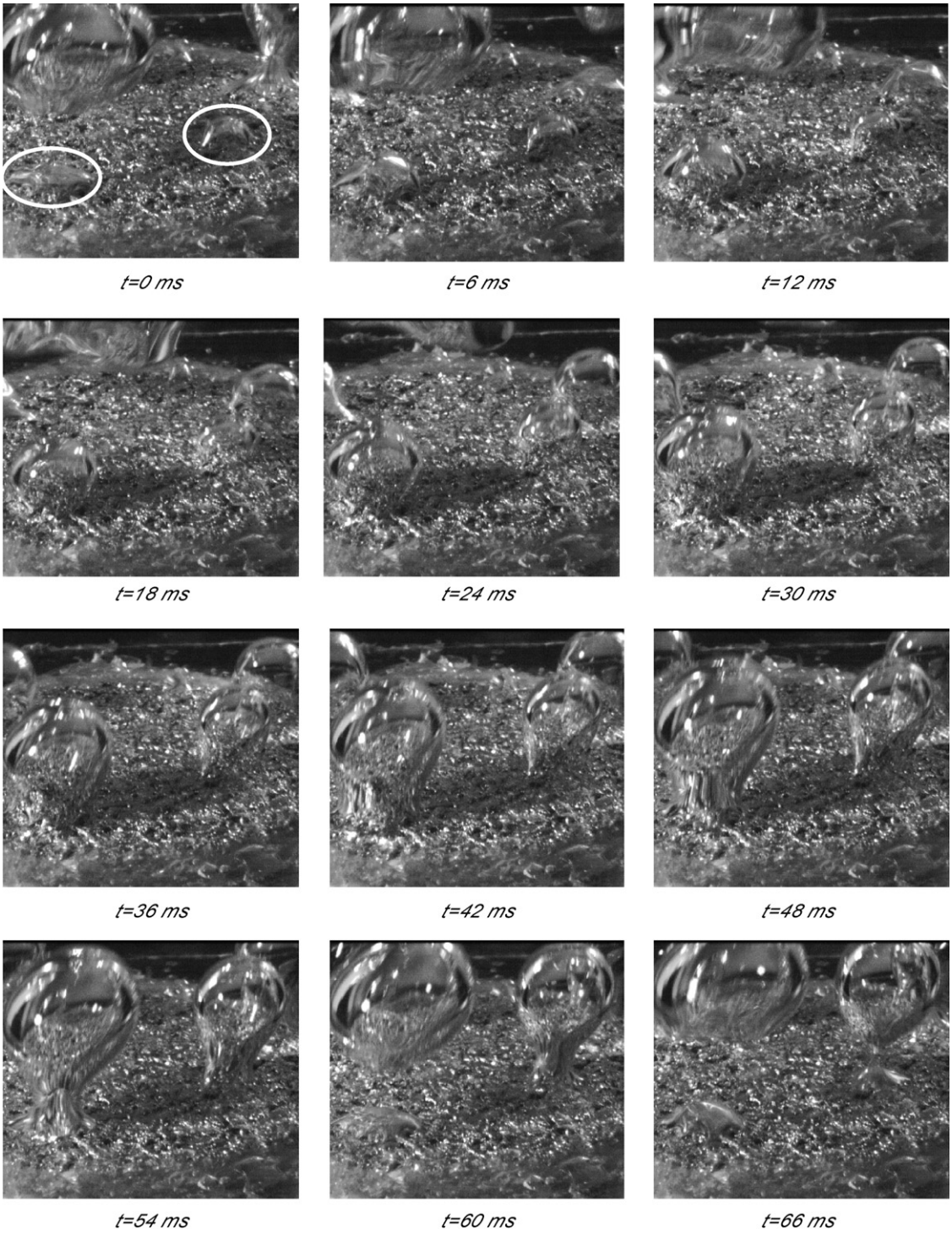

Fig. 15. Instances of bubble formation at two different sparger regions.

actions between the bubbles directly onto or in the vicinity of the porous sparger region are of great interest and should be further studied.

3.7. Mean Sauter diameter of bubbles

To the authors' best knowledge, there is a lack of correlations for predicting the size of bubbles formed from a porous sparger. Thus, an attempt was made to formulate a correlation based on dimensional analysis for the prediction of the mean Sauter diameter of the bubbles formed from a porous sparger at the homogeneous regime. This correlation includes the most important of the aforementioned parameters that affect the *initial* bubble size, namely:

- the gas phase *superficial velocity*,
- the *physical properties* of the liquid phase (i.e., surface tension, viscosity, density),

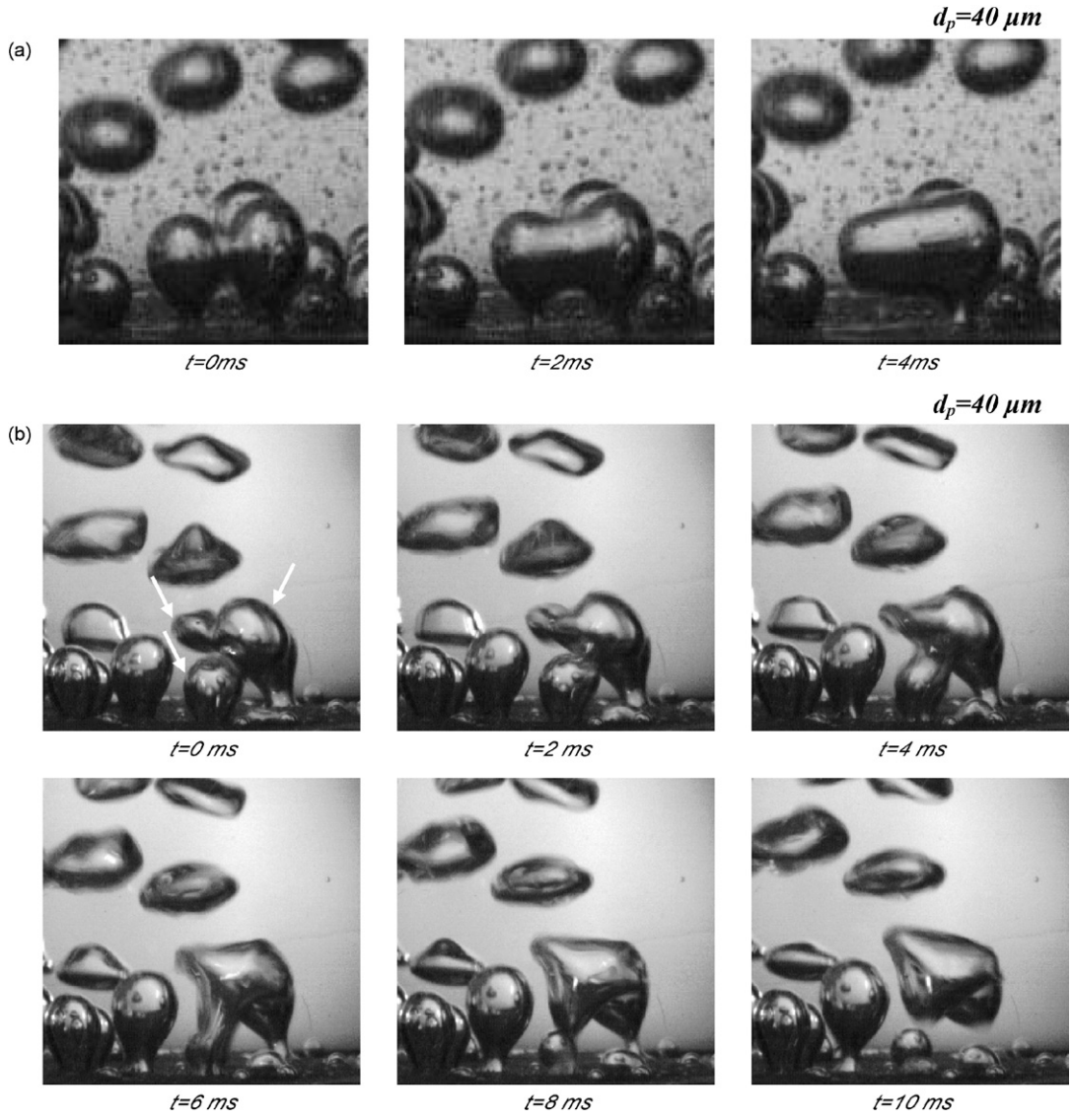

Fig. 16. Instances of bubble coalescence during their formation (d_p = 40 μm) in: (a) glycerin solution and (b) water.

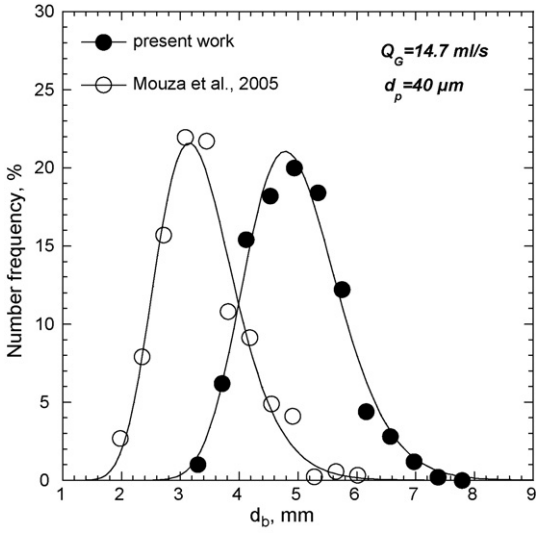

Fig. 17. Bubble size distribution for water (Q_G = 14.7 ml/s and d_p = 40 μm).

- the *sparger diameter* and
- the *sparger mean pore size*.

The non-dimensional numbers used in the correlation are the *Froude* (*Fr*), *Weber* (*We*) and *Reynolds* (*Re*) defined as follows:

$$Fr = \frac{U_{GS}^2}{d_s g} \tag{7}$$

$$We = \frac{\rho_L U_{GS}^2 d_s}{\sigma_L} \tag{8}$$

$$Re = \frac{\rho_L U_{GS} d_s}{\mu_L} \tag{9}$$

where U_{GS} is the gas superficial velocity based on the sparger surface, d_s the sparger diameter and ρ_L, μ_L and σ_L are the liquid density, viscosity and surface tension, respectively. Finally, the ratio of the sparger mean pore size to sparger diameter (d_p/d_s) was also included to account for the different porous sparger

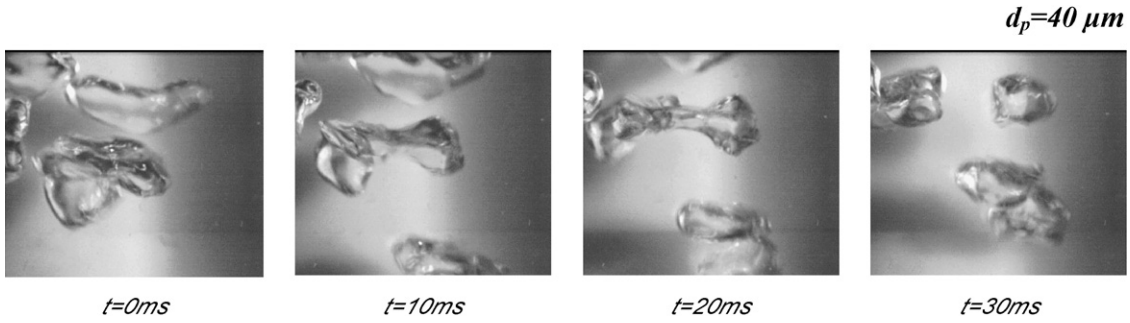

Fig. 18. Instances of bubble breakage 3 cm above the sparger for water.

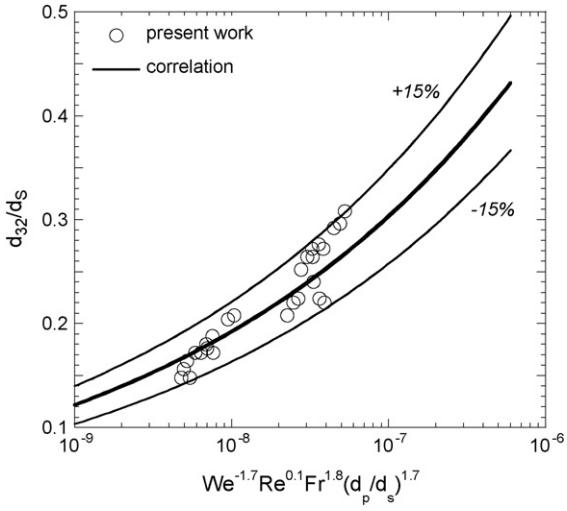

Fig. 19. Comparison of the initial Sauter diameter prediction with experimental data.

characteristics. The correlation has the form:

$$\frac{d_{32}}{d_s} = 7.35\left[We^{-1.7}\,Re^{0.1}\,Fr^{1.8}\left(\frac{d_p}{d_s}\right)^{1.7}\right]^{1/5} \tag{10}$$

where d_{32} is the mean Sauter diameter. This correlation is plotted in Fig. 19 and it is in very good agreement (±15%) with all experimental data. This correlation is good when stainless steel porous spargers are employed, but considering the findings of Koide et al. [25] it may be also applicable for all metal porous spargers.

4. Concluding remarks

In bubble column reactor design the homogeneous regime is usually the most desirable, because it enhances the efficiency of the equipment by providing a greater gas–liquid interfacial area. For this case, new data concerning initial bubble size distributions and mean Sauter diameters in a small bubble column equipped with two different porous spargers are presented for a number of liquids covering a wide range of surface tension and viscosity values.

By taking into consideration the forces acting on an under-formation bubble, i.e., the upward acting forces (buoyancy, gas momentum and gas pressure force) and the resistance to bubble formation (drag, inertial and surface tension force), it can be concluded that the bubble development is controlled by the pore size distribution, the gas flow rate and the properties of the liquid phase. The characteristics of the bubbles, i.e., number and size distribution, are the combined effect of all the above factors that can influence one or even all the forces acting on an under-formation bubble. For example, for a given gas flow rate and sparger pore size, a high viscosity value seems to favor the activation of more pores and thus the formation of more numerous and smaller bubbles, but the same result can be obtained when a low-surface tension liquid is employed, because in this case the force that keeps the bubble attached to the sparger decreases.

A new correlation for the prediction of the bubble mean Sauter diameter from this kind of sparger has been proposed and found to be in reasonably good agreement with all experimental data. Moreover, the implementation of the initial bubble size distribution and/or the Sauter diameter into a commercial *CFD* code can render it to a powerful tool for the simulation of bubble column operation and thus improve the physical understanding of its hydrodynamic behavior.

In addition, meticulous visual observations of the bubble formation process on the porous sparger indicate that many neighboring pores contribute to a single bubble production. It is also proved that bubble size in bubble columns equipped with porous sparger depends extensively on phenomena occurring directly onto or in the vicinity of the sparger surface. Consequently, experiments in microscopic scale focused on the phenomena occurring onto the sparger surface are needed. Moreover, in order to establish rigorous criteria for the coalescence and breakage of fluid objects at the microscopic level, more experimental data as well as theoretical analyses are required.

Acknowledgements

The authors wish to acknowledge the expertise of the Laboratory technicians Mr. A. Lekkas and Mr. T. Tsilipiras as well as the CPERI for the use of the SEM.

References

[1] K.M. Sutherland, D.T. Pearsonl, L.S. Gordon, Independent control of blood gas Po_2 and Pco in a bubble oxygenator, Clin. Phys. Physiol. Meas. 9 (2) (1998) 97–105.
[2] E. Camarasa, C. Vial, S. Poncin, G. Wild, N. Midoux, J. Bouillard, Influence of coalescence behaviour of the liquid and of gas sparging on hydrody-

namics and bubble characteristics in a bubble column, Chem. Eng. Proc. 38 (4–6) (1999) 329–344.
[3] G. Hebrard, D. Bastoul, M. Roustan, Influence of gas sparger on the hydrodynamic behaviour of bubble columns, Trans. Inst. Chem. Eng. 74 (1996) 406–414.
[4] J.B. Joshi, V.S. Vitankar, A.A. Kulkarni, M.T. Dhotre, K. Ekambara, Coherent flow structures in bubble column reactors, Chem. Eng. Sci. 57 (16) (2002) 3157–3183.
[5] K.M. Dhanasekharan, J. Sanyal, A. Jain, A. Haidari, A generalized approach to model oxygen transfer in bioreactors using population balances and computational fluid dynamics, Chem. Eng. Sci. 60 (1) (2005) 213–218.
[6] T.J. Jones, D.D. Deal, J.C. Vernon, N. Blackburn, D.A. Stump, How effective ere cardiopulmonary bypass circuits at removing gaseous microemboli? J. Am. Soc. Extra-Corpor. Tech. 34 (2002) 34–39.
[7] Y.T. Shah, B.G. Kelkar, S.P. Godbole, W.-D. Deckwer, Design parameters estimations for bubble column reactors, AIChE J. 28 (3) (1982) 353–379.
[8] M. Kaji, T. Sawai, K. Mori, M. Iguchi, Behaviors of bubble formation from a bottom porous nozzle bath, in: Proceedings of the 5th ExHFT, Thessaloniki, Greece, 2001.
[9] D. Pfleger, S. Becker, Modelling and simulation of the dynamic flow behaviour in a bubble column, Chem. Eng. Sci. 56 (4) (2001) 1737–1747.
[10] P.M. Wilkinson, A.P. Spek, L.L. Vandierendonck, Design parameters estimation for scale-up of high-pressure bubble-columns, AIChE J. 38 (4) (1992) 544–554.
[11] G. Wild, H.Z. Li, S. Poncin, E. Olmos, Some aspects of the hydrodynamics of bubble columns, Int. J. Chem. React. Eng. 1 (2003) 1–36.
[12] V.V. Buwa, V.V. Ranade, Dynamics of gas–liquid in a rectangular bubble column: experiments and single/multi-group CFD simulations, Chem. Eng. Sci. 57 (22–23) (2002) 4715–4736.
[13] F. Lehr, M. Millies, D. Mewes, Bubble-size distributions and flow fields in bubble columns, AIChE J. 48 (11) (2002) 2426–2443.
[14] S. Lo, Application of population balance to CFD modelling of gas–liquid reactors, in: Proceedings of Conference on Trends in Numerical and Physical Modelling for Industrial Multiphase Flows, Corse, 27–29 September, 2000.
[15] E. Olmos, C. Gentric, Ch. Vial, G. Wild, N. Midoux, Numerical simulation of multiphase flow in bubble column reactors. Influence of bubble coalescence and break-up, Chem. Eng. Sci. 56 (21–22) (2001) 6359–6365.
[16] K. Shimizu, S. Takada, K. Minekawa, Y. Kawase, Phenomenological model for bubble column reactors: prediction of gas hold-ups and volumetric mass transfer coefficients, Chem. Eng. J. 78 (1) (2000) 21–28.
[17] D. Colella, D. Vinci, R. Bagatin, M. Masi, E.A. Bakr, A study of coalescence and breakage mechanisms in three different bubble columns, Chem. Eng. Sci. 54 (21) (1999) 4767–4777.
[18] P.L.C. Lage, R.O. Esposito, Experimental determination of bubble size distributions in bubble columns: prediction of mean bubble diameter and gas holdup, Powder Technol. 101 (2) (1999) 142–150.
[19] R. Pohorecki, W. Moniuk, P. Sobieszuk, G. Dabrowiecki, Bubble diameter correlation via numerical experiment, Chem. Eng. J. 113 (1) (2005) 35–39.
[20] P. Wongsuchoto, T. Charinpanitkul, P. Pavasant, Bubble size distribution and gas–liquid mass transfer in airlift contactors, Chem. Eng. J. 92 (1–3) (2003) 81–90.
[21] M. Polli, M. Stanislao, R. Bagatin, E.A. Bakr, M. Masi, Bubble size distribution in the sparger region of bubble columns, Chem. Eng. Sci. 57 (1) (2002) 197–205.
[22] R. Parthasarathy, N. Ahmed, Size distribution of bubbles generated by fine-pore spargers, J. Chem. Eng. Jpn. 29 (6) (1996) 1030–1034.
[23] G. Keitel, U. Onken, Inhibition of bubble coalescence by solutes in air/water dispersions, Chem. Eng. Sci. 37 (11) (1982) 1635–1638.
[24] T. Miyahara, A. Tanaka, Size of bubbles generated from porous plates, J. Chem. Eng. Jpn. 30 (2) (1997) 353–355.
[25] K. Koide, S. Kato, Y. Tanaka, H. Kubota, Bubbles generated from porous plate, J. Chem. Eng. Jpn. 1 (1) (1968) 51–56.
[26] A.A. Mouza, G.K. Dalakoglou, S.V. Paras, Effect of liquid properties on the performance of bubble column reactors with fine pore spargers, Chem. Eng. Sci. 60 (5) (2005) 1465–1475.
[27] B. Bowonder, R. Kumar, Studies in bubble formation-IV: bubble formation at porous discs, Chem. Eng. Sci. 25 (1) (1970) 25–32.
[28] G. Houghton, A.M. McLean, P.D. Ritchie, Mechanism of formation of gas bubble-beds, Chem. Eng. Sci. 7 (1–2) (1957) 40–50.
[29] W.D. Deckwer, Bubble Column Reactors, John Wiley and Sons, England, 1992.
[30] T. Loimer, G. Machu, U. Schaflinger, Inviscid bubble formation on porous plates and sieve plates, Chem. Eng. Sci. 59 (4) (2004) 809–818.
[31] P. Snabre, F.I. Magnifotcham, Formation and rise of a bubble stream in a viscous liquid, Eur. Phys. J. B 4 (1998) 369–377.
[32] R. Schafer, C. Merten, G. Eigenberger, Bubble size distribution in a bubble column reactor under industrial conditions, Exp. Therm. Fluid Sci. 26 (6–7) (2002) 595–604.
[33] J. Zahradnik, M. Fialova, V. Linek, The effect of surface-active additives on bubble coalescence in aqueous media, Chem. Eng. Sci. 54 (21) (1999) 4757–4766.
[34] K. Tse, T. Martin, C.M. McFarlane, A.W. Nienow, Small bubble formation via a coalescence dependent break-up mechanism, Chem. Eng. Sci. 58 (2) (2003) 275–286.